Thickness-dependent atomic structures of two-dimensional few-layer ZnO: A density functional theory study

Dong Han [1,*] Xian-Bin Li [2] Nian-Ke Chen,[2] Dan Wang,[3] Sheng-Yi Xie [4] Xue-Jiao Chen,[5] and De-Zhen Shen[1,†]

[1]*State Key Laboratory of Luminescence and Applications, Changchun Institute of Optics, Fine Mechanics and Physics, Chinese Academy of Sciences, Changchun 130033, People's Republic of China*

[2]*State Key Laboratory of Integrated Optoelectronics, College of Electronic Science and Engineering, Jilin University, Changchun 130012, People's Republic of China*

[3]*School of Materials Science and Engineering, Beijing Institute of Technology, Beijing 100081, People's Republic of China*

[4]*School of Physics and Electronics, Hunan University, Changsha 410082, People's Republic of China*

[5]*CAS Key Laboratory of Magnetic Materials, Devices and Zhejiang Province Key Laboratory of Magnetic Materials and Application Technology, Ningbo Institute of Materials Technology and Engineering, Chinese Academy of Sciences, Ningbo 315201, People's Republic of China*

(Received 24 July 2023; accepted 5 January 2024; published 19 January 2024)

The thickness-dependent atomic structures of two-dimensional (2D) few-layer (FL) ZnO are systematically investigated by the first-principles calculations. It is found that the structural transformation between thinner FL ZnO with graphitic structure (FL *g*ZnO) and thicker FL ZnO with wurtzite structure (FL *w*ZnO) takes place at the critical thickness of 9–12 Zn-O atomic layers. At the thickness of 9–12 layers, both graphitic and wurtzite structures can coexist at room temperature. In FL *g*ZnO, the interlayer interaction is a long-range Coulomb interaction, and the charge population of Zn and O inside does not change during the structural transformation. Moreover, we demonstrate that the structural transformation of FL ZnO originates from the competition between the high energy of the O $2p_z$ orbital in the graphitic structure and the polar-surface-induced dipole energy in the wurtzite structure. Our microscopic understanding guides a clear direction of regulating the atomic structure of FL ZnO, further optimizing its electronic properties, which benefits developing function-advanced 2D stacked devices.

DOI: 10.1103/PhysRevB.109.014105

I. INTRODUCTION

For a semiconductor material, understanding its atomic structure is of fundamental importance since it highly determines the unique property of the semiconductor material. For example, zinc oxide (ZnO) has attracted tremendous research attention due to its excellent optoelectronic and piezoelectric properties, which exhibits extraordinary potential in a wide range of applications, such as light-emitting diodes [1–3], low-threshold lasing [4,5], and piezoelectric devices [6]. ZnO crystal exists in two bulk phases, hexagonal wurtzite and cubic zinc blende, at ambient conditions [7]. Both phases have the same local tetrahedral coordination. Every Zn is tetrahedrally bonded with O and vice versa. However, their structural discrepancy in the bond angle of the second-nearest neighbors leads to significant differences in their piezoelectric characteristic [8,9]. Besides that, the denser rocksalt phase obtained at high pressure, which has the local sixfold coordination, possesses an indirect band gap [10–12], unlike the direct-band-gap characteristic found in ZnO with both wurtzite and zinc blende phases [12,13]. Moreover, the rocksalt phase is a centrosymmetric structure; therefore it does not possess the piezoelectric property. In recent years, various nanomorphologies of ZnO [14–17], combined with its advantages of low cost, environmental friendliness, and easy synthesis, have become the ideal candidate materials for scientific research and industrial applications in nanotechnology. Before exploiting the unique properties of ZnO-based nanomorphologies, it is important to investigate the low-dimensional atomic structures of them first and comprehensively.

When bulk ZnO (BK ZnO) with wurtzite phase shrinks to a few atomic layers in [0001] direction, becoming a two-dimensional (2D) material, its atomic structure transforms from wurtzite to graphitic (or graphene-like, hexagonal boron nitride-like) geometry. This structural transformation has been extensively demonstrated by both theory and experiment [18–23]. However, the atomic structure of few-layer ZnO (FL ZnO), especially around the critical atomic layers for structural transformation, is still not fully understood. For example, the theoretical calculations predicted the wurtzite-to-graphitic transformation takes place at over ten-layer thickness [19,20], but experiments indicate the graphitic structure is more stable only when the thickness of FL ZnO is less than four layers [21–23]. Moreover, the structural transformation is strongly sensitive to many factors, such as external strain [20,24], substrate [24], and doping [25], which makes the atomic structure of FL ZnO even more complicated. In recent years, a large number of large-scale FL ZnO with graphitic structure (FL

*hand@ciomp.ac.cn
†shendz@ciomp.ac.cn

*g*ZnO) samples have been synthesized successfully [26–28], which also exhibits its superior performance [29–31]. Therefore, understanding the atomic structure of FL ZnO becomes highly urgent, especially from a microscopic perspective, which is necessary to further improve its performance for function-advanced 2D stacked devices.

In this work, based on the first-principles calculations, we have comprehensively studied the atomic structures of FL ZnOs with thickness varying from 2 to 15 layers. We found that, thinner than 9 Zn-O atomic layers, FL ZnO always possesses the graphitic structure, and thicker than 12 layers, FL ZnO prefers the wurtzite structure. The structural transformation of FL ZnO takes place at the thickness of 9–12 layers, and at this thickness, both graphitic and wurtzite structures can coexist at room temperature. Unlike the van der Waals interaction normally found in layered materials, the interlayer interaction in FL *g*ZnO is a long-range Coulomb interaction, and the charge population of Zn and O inside FL ZnO does not change during the structural transformation. Our calculations demonstrated that the structural transformation originates from the competition between the high energy of O $2p_z$ orbital in FL *g*ZnO and the polar-surface-induced dipole energy in FL ZnO with wurtzite structure (FL *w*ZnO). This microscopic understanding offers a clear direction for adjusting the atomic structure of FL ZnO and further optimizing its electronic properties for developing function-advanced stacked 2D devices.

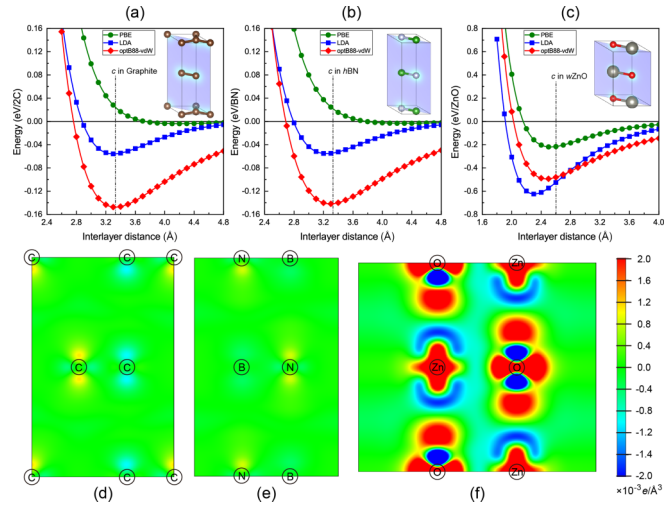

FIG. 1. Binding energies as a function of interlayer distance in (a) graphite, (b) *h*BN, and (c) BK *g*ZnO. The insets show their unit cells, respectively. The total energies of them in their monolayer forms are set to zero, respectively. The dashed lines show the lattice constant c of the optimized unit cell of graphite, *h*BN, and BK *w*ZnO, respectively. The 2D slice (light-blue slice in unit cells) of the charge-density difference of (d) graphite, (e) *h*BN, and (f) BK *g*ZnO between when the layers adjoin at their equilibrium distances and the corresponding isolated layers. The position of atoms on 2D slices are labeled in each material, respectively. (The VESTA software package was used to generate all figures [50].)

II. COMPUTATIONAL METHODS

Our first-principles calculations were carried out based on the density functional theory (DFT) [32,33] as implemented in the VASP codes [34,35]. Projector augmented-wave (PAW) potentials [36] were used to describe the core electrons, and the cutoff energy for the plane-wave basis was set to 540 eV. We employed the Perdew-Burke-Ernzerhof (PBE) functional [37] for evaluating the exchange-correlation energy and the optB88-vdW functional [38] for correcting the van der Waals interactions. According to this setup, the calculated lattice constant $a = b = 3.268$ Å, $c/a = 1.618$, of BK ZnO with wurtzite structure (BK *w*ZnO) is only 0.5%, 1.0% larger than the experiment [39]. In this calculated unit cell of BK *w*ZnO, the z-directional displacement between the intralayer Zn and O, $R_1 = 0.644$ Å, and the z-directional displacement between the interlayer Zn and O, $R_2 = 2.000$ Å, as illustrated in Fig. S1 in the Supplemental Material (SM) [40]. We used the supercell approach to model FL ZnO. The supercell with a layer-dependent L_a ($= L_b$) and a fixed L_c (40 Å for 2–13 layers, 50 Å for 14 and 15 layers) includes FL ZnO with a 1×1 unit cell for $L_a \times L_b$ and layers varying from 2 to 15 layers (13-layer thickness: $\approx$ 31 Å, 15-layer thickness: $\approx$ 36 Å) for L_c. All atoms inside could relax until the Hellmann-Feynman forces on individual atoms were less than 0.03 eV/Å. The $9 \times 9 \times 1$ Monkhorst-Pack mesh grids were used for k-point sampling in the Brillouin zone. To calculate energy barriers between different atomic geometries, the climbing image–nudged elastic band (CI-NEB) method [41] was used with eight images, including the optimized initial and final geometries. The projected density of states (PDOS) and Mulliken population analysis were processed with the LOBSTER program [42–46], based on the VASP calculations.

III. RESULTS AND DISCUSSION

We first concern the interlayer interaction in FL *g*ZnO. Normally in 2D layered materials, the intermediate-range van der Waals interaction greatly affects its properties. Therefore the exchange-correlation functionals in DFT calculations need to be carefully selected to accurately describe this intermediate-range interaction. Figure 1 shows the binding energy as a function of interlayer distance and the charge transfer between layers in BK ZnO with graphitic structure (BK *g*ZnO), including that in graphite and hexagonal BN (*h*BN) as a comparison. For layered materials in DFT calculations, the PBE functional hardly presents the weak van der Waals interaction, while the local density approximation (LDA) functional always overestimates this interaction strength [47], which is clearly shown in Figs. 1(a) and 1(b). In graphite and *h*BN, there are almost no binding energies in the DFT-PBE calculations and only 0.06 eV/2C for graphite and 0.05 eV/BN for *h*BN in DFT-LDA calculations, respectively. When taking account of the van der Waals interaction in the optB88-vdW functional, the binding energy noticeably increases to 0.15 eV/2C for graphite and 0.14 eV/BN for *h*BN, respectively, indicating that the van der Waals force is the dominate interaction in these layered materials. However, the binding energy in BK *g*ZnO is completely different from that in graphite and *h*BN. In Fig. 1(c) it is clearly found that the binding energy is no longer close to zero but is as large as 0.22 eV/ZnO in the DFT-PBE calculation and

overestimated to 0.62 eV/ZnO in the DFT-LDA calculation. The binding energy of 0.49 eV/ZnO in the DFT-optB88-vdW calculation is smaller than that in DFT-LDA calculation, indicating no noteworthy van der Waals interaction between the layers. From the perspective of binding-energy calculations, it is concluded that the interlayer interaction in BK *g*ZnO, as well as in FL *g*ZnO, is not the same as the van der Waals interaction in the layered materials. Furthermore, the equilibrium layer distance of 2.303 Å in BK *g*ZnO is a little smaller than the corresponding distance $R_1 + R_2$ of 2.644 Å in BK *w*ZnO, shown in Fig. S1 in the Ref. [40]. This layer distance is much smaller than the van der Waals–interaction distance of over 3.2 Å in graphite and *h*BN, which further reveals the strong interlayer bonding interaction in BK *g*ZnO, as well as in FL *g*ZnO. Figures 1(d)–1(f) show that the charge density redistributes when the atomic layers are close to each other in graphite, *h*BN, and BK *g*ZnO, respectively. In graphite and *h*BN, there is no obvious charge redistribution, while in BK *g*ZnO, the electron charge significantly redistributes around the ions of Zn and O when the isolated layers adjoin at its equilibrium distance. This charge redistribution indicates the strong Coulomb interaction between the layers in BK *g*ZnO and further reveals the Coulomb interaction between layers in FL *g*ZnO.

To understand the atomic structure of FL ZnO varies along with the thickness, both graphitic and wurtzite structures are used as the initial structures to optimize the stable geometries of FL ZnOs. Figure 2 shows the equilibrium lattice constants a and the z-directional displacement R_1 between the intralayer Zn and O of the FL ZnOs from 2 to 15 layers. The larger R_1 (the higher bar) illustrates that the more the optimized geometry looks like the wurtzite structure and contrarily looks like the graphitic structure. It is clearly found that the graphitic structure is always stable when FL ZnOs vary across from 2 to 15 layers, while the wurtzite structure appears only when the FL ZnOs are thicker than eight layers. As shown in Fig. 1(a), the equilibrium lattice constants a^G of FL *g*ZnOs are generally larger than the a^W of FL *w*ZnOs. Moreover, the a^G exhibits a gentle increase from 3.342 Å to 3.408 Å to 3.424 Å along with the layer of FL *g*ZnO increases from 2 to 9 to 15 layers. In contrast, the a^W exhibits a gradual decrease from 3.316 to 3.287 Å along with the layer of FL *w*ZnO increases from 9 to 15 layers. As shown in Fig. 2(b), mostly due to the larger a^G, the thickness of FL *g*ZnO is generally smaller than that of FL *w*ZnO at the same layer. For example, the thickness of FL ZnO with graphitic and wurtzite structures is 32.6 and 36.3 Å at 15 layers, respectively. For these FL ZnOs, the R_1 at surface is visibly different from that inside, namely, the larger R_1 at the surface in the graphitic structure and the smaller R_1 at the surface in the wurtzite structure. This indicates the R_1 inside is the consequence of the Coulomb interaction with two-side nearby layers, where only one-side Coulomb interaction makes R_1 at the surface be different. It also suggests R_1 at the surface as well as the structure of FL ZnO is sensitive to the external factors interacting with the surface. Moreover, for the FL *w*ZnO, R_1 generally increases along with increasing the thickness of FL *w*ZnO. The average R_1 inside increases from 0.45 Å (69% of R_1 in BK *w*ZnO) to 0.57 Å (89% of R_1 in BK *w*ZnO). From this point of view, the Coulomb interaction between the atomic layers is a long-range interaction in FL ZnO.

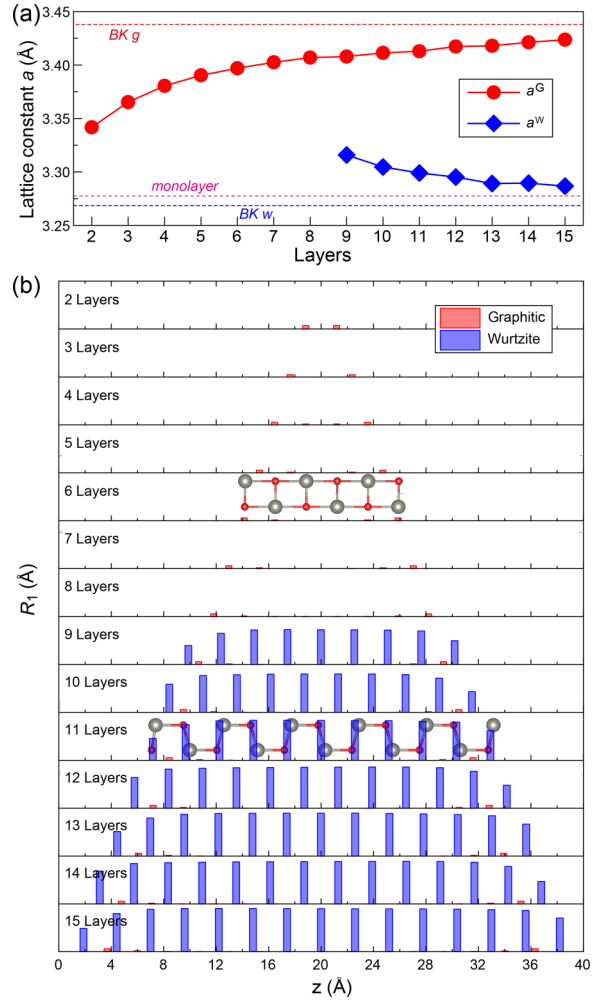

FIG. 2. (a) The equilibrium lattice constants a of FL ZnOs (a^G, a^W for graphitic and wurtzite structures) vary along with the layers from 2 to 15 layers. The equilibrium lattice constants a of BK *g*ZnO, monolayer ZnO, and BK *w*ZnO are shown in red, pink, and blue dashed lines, respectively. (b) The z-directional displacement R_1 between the intralayer Zn and O in FL ZnOs from 2 to 15 layers. The height of the bar is the z-directional displacement R_1, where the scale of Y axis varies from 0 (R_1 in BK *g*ZnO) to 0.644 Å (R_1 in BK *w*ZnO). The bar located in the X axis stands the average z-directional position of the Zn-O layer in the supercell model. Two corresponding optimized atomic structures are illustrated in the 6 and 11 layers.

We also compared the energies of FL ZnOs with different atomic structures. Figure 3(a) shows the average binding energies of FL ZnOs with graphitic and wurtzite structures vary along with their layers. The average binding energy (E_b) is defined as $E_b = \frac{E_{\rm tot}^{FL\,{\rm ZnO}}(n) - nE_{\rm tot}^{\rm mono\,ZnO}}{n}$, where $E_{\rm tot}^{FL\,{\rm ZnO}}$ and $E_{\rm tot}^{\rm mono\,ZnO}$ are the total energies of FL ZnO including n atomic layers and the total energy of monolayer ZnO with graphitic structure, respectively. It is clearly found the E_bs of FL ZnOs generally increase (more negative) along with the layers, which further proves the interlayer Coulomb interaction in FL ZnO is the long-range interaction. When FL ZnOs are thinner than nine layers, only the graphitic structure is stable and the E_bs of FL *g*ZnOs increases from –0.26 eV/ZnO for two layers to –0.49 eV/ZnO for eight layers. Thicker than

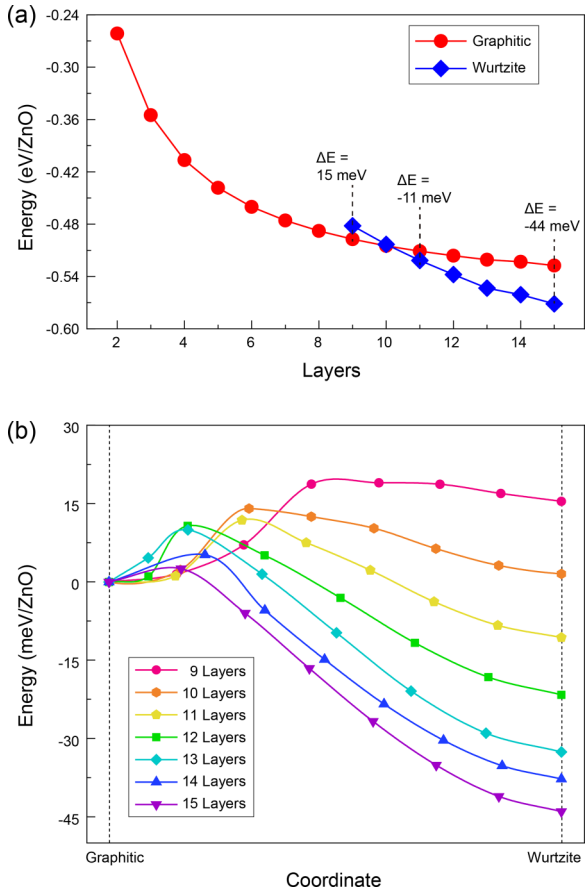

FIG. 3. (a) The average binding energies (E_b) of FL ZnOs with graphitic and wurtzite structures vary along with the layers, respectively. The total energy of monolayer ZnO is set to zero. (b) The energy barriers of FL ZnOs between graphitic and wurtzite structures as a function of the layers. FL ZnO with graphitic geometry is set to zero.

eight layers, the E_bs of FL *w*ZnOs exhibit the more noticeable increase than that of FL *g*ZnOs. The E_b of FL *w*ZnO is only 15 meV/ZnO smaller than that of FL *g*ZnO at nine layers, and they have the same E_bs of –0.50 meV/ZnO at ten layers. Thicker than ten layers, FL *w*ZnOs always have larger average binding energies than FL *g*ZnOs. Their E_b's difference increases from 11 meV/ZnO for 11 layers to 44 meV/ZnO for 15 layers. Because both graphitic and wurtzite structures are stable when FL ZnO is thicker than 8 layers, we calculated the energy barriers of FL ZnOs between graphitic and wurtzite structures varying from 9 to 15 layers, as shown in Fig. 3(b). The energy barriers for structural transformation between graphitic and wurtzite structures are no more than 33 meV/ZnO when FL ZnOs have 9–12 atomic layers. When FL ZnOs are thicker than 12 layers, due to the larger average binding energy in wurtzite structures, the energy barriers for structural transformation from graphitic to wurtzite structures are only 10.0 meV/ZnO for 13 layers, 5.2 meV/ZnO for 14 layers, and 2.5 meV/ZnO for 15 layers, respectively, while the energy barriers for structural transformation from wurtzite to the graphitic structures are as large as 42.5 meV/ZnO, 42.9 meV/ZnO, and 46.5 meV/ZnO, respectively. Therefore, considering the kinetic energy of ∼25.7 meV at room temperature, both graphitic and wurtzite structures exist in FL ZnOs with a thickness of 9–12 layers. But only wurtzite structure is in existence when FL ZnOs are thicker than 12 layers.

In order to explore the origin of structural transformation between FL ZnOs with graphitic and wurtzite structures, we first analyzed the Mulliken population in BK *g*ZnO, BK *w*ZnO, FL *g*ZnO, and FL *w*ZnO, as shown in Table I. In general, the electron's donation and acceptance appear between the Zn 4*s* orbital and O 2*p* orbital, because Zn 3*d* and O 2*s* orbitals are buried deeply in the valance band of the ZnO's band structure. In both BK *g*ZnO and BK *w*ZnO, more than 1.4*e* are donated from the Zn 4*s* orbital and more than 1.5*e* are accepted by the O 2*p* orbital. The same amount of donating and accepting electrons indicates the local structural variation has little effect on that. Similarly, inside FL *g*ZnO and FL *w*ZnO, the same 1.4*e* are donated from the Zn 4*s* orbital and the same 1.5*e* are accepted by the O 2*p* orbital. However, for the surfaces of FL ZnOs, the electron's donation and acceptance are obviously different. In FL *g*ZnO, Zn at the $(0001)^*$ surface and O at the $(000\bar{1})^*$ surface have almost the same amount of donating and accepting electrons as inside Zn and O does. Moreover, only a little of the negative charge is accumulated at surfaces. But in FL *w*ZnO, the 4*s* orbital of Zn at the (0001) surface donates less than 1.2*e*, and the 2*p* orbital of O at the $(000\bar{1})$ surface accepts a little more than 1.4*e*. As a result, an average charge of 0.16*e* is accumulated at polar surfaces. Furthermore, we analyzed the Zn-and-O-orbital energy levels of FL ZnOs, as shown in Fig. 4. The orbital energy levels are the weighted average of PDOS in Fig. S2 in the Ref. [40]. For the BK ZnOs, the largest difference in the orbital energy levels is the O 2*p* orbital, where the energy of the $2p_z$ orbital is obviously higher than that of the $2p_x$ and $2p_y$ orbitals in BK *g*ZnO, while the energies of the $2p_z$, $2p_x$, and $2p_x$ orbitals are almost the same in BK *w*ZnO, due to the local structural symmetry. The energy difference of the O $2p_z$ orbital between in BK *g*ZnO and in BK *w*ZnO is 0.33 eV, which is consistent with the energy difference of 0.14 eV/ZnO between two phases. Similar to the Mulliken population analysis, the orbital energies of Zn and O inside FL ZnOs are the same as that in BK ZnOs. For surface Zn in FL ZnOs, the energies of the Zn 4*s* and 3*d* orbitals in FL *g*ZnO are nearly the same as those in BK *g*ZnO, while the energies of Zn 4*s* and 3*d* orbitals in FL *w*ZnO are evidently lower than those in BK *w*ZnO. For surface O in FL ZnOs, the energies of O 2*p* orbitals are almost the same. Both show the energy of the $2p_z$ orbital is higher than that of the $2p_x$ and $2p_y$ orbitals, because of the nonbonding $2p_z$ orbital of surface O in FL *w*ZnO. As a result, stabler *w*ZnO exhibits lower orbital energies at the surface (FL *w*ZnO) than the *g*ZnO does (FL *g*ZnO). Therefore the orbital energies at the surface cannot contribute to the structural transformation between the FL ZnOs with graphitic and wurtzite structures. As is discussed above, the surface of FL *w*ZnO accumulates charge, forming a dipole between two surfaces. The dipole induces an internal electric field that holds a dipole energy, as shown in Fig. S3 in the Ref. [40]. For example, for 11-layer FL *w*ZnO, the dipole energy is estimated to be 0.73 eV, shown in Table S1 in the Ref. [40]. This dipole energy of 0.73 eV is close to the energy drop of 1.4 eV in 11-layer BK ZnOs between the graphitic and

TABLE I. The Mulliken population analysis in BK *g*ZnO, BK *w*ZnO, FL *g*ZnO (11 layers), and FL *w*ZnO (11 layers). The negative Δe stands for donating electrons, and the positive Δe stands for accepting electrons. The surfaces for Mulliken population analysis are labeled in Fig. S3 in the Ref. [40].

		Mulliken population $\|e\|$								
		Zn 4*s*		Zn 3*d*		O 2*p*		O 2*s*		Total
Structure	Location	Mull. Pop.	Δe	Mull. Pop.	Δe	Mull. Pop.	Δe	Mull. Pop.	Δe	Δe
BK *g*ZnO	Bulk	0.58	–1.42	9.99	–0.01	5.51	+1.51	1.92	–0.08	0
BK *w*ZnO	Bulk	0.56	–1.44	10.00	0.00	5.53	+1.53	1.92	–0.08	0.01
FL *g*ZnO	*Inside*	0.58	–1.42	9.99	–0.01	5.51	+1.51	1.92	–0.08	0
	(0001)* *Surface*	0.55	–1.45	9.98	–0.02	5.47	+1.47	1.92	–0.08	–0.08
	$(000\bar{1})$* *Surface*	0.55	–1.45	9.98	–0.02	5.48	+1.48	1.93	–0.07	–0.06
FL *w*ZnO	*Inside*	0.57	–1.43	10.00	0.00	5.53	+1.53	1.92	–0.08	0.02
	(0001) *Surface*	0.78	–1.22	9.98	–0.02	5.43	+1.43	1.94	–0.06	0.13
	$(000\bar{1})$ *Surface*	0.53	–1.47	9.93	–0.07	5.43	+1.43	1.92	–0.08	–0.19

wurtzite phases when one Zn-O layer is assumed to be equal in energy to the surface layer. More importantly, the dipole energy in FL *w*ZnO is increasing more gently than the energy increment due to the O $2p_z$ orbital along with increasing the thickness of FL *g*ZnO. Therefore, it can be concluded that the structural transformation of FL ZnO is the competition between the high energy of the O $2p_z$ orbital in FL *g*ZnO and the polar-surface-induced dipole energy in FL *w*ZnO.

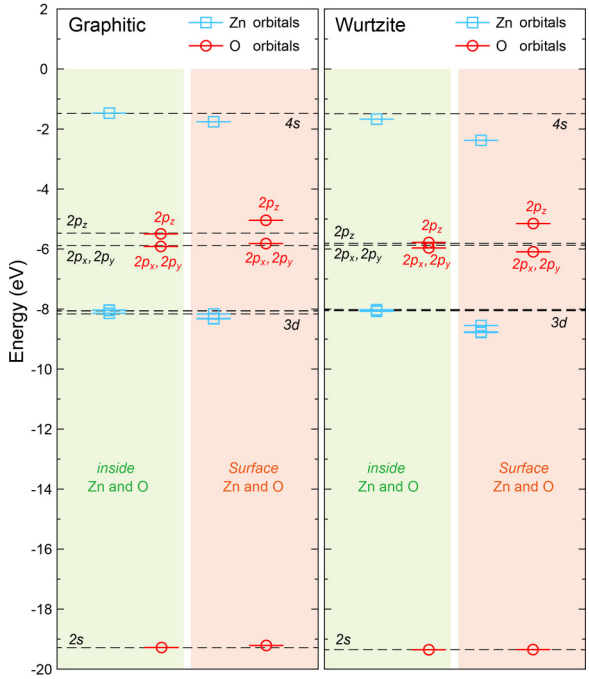

FIG. 4. The Zn- and O-orbital energy levels (cyan and red) of FL *g*ZnO and FL *w*ZnO (11 layers). The dashed lines are the corresponding orbital energy levels calculated in BK *g*ZnO and BK *w*ZnO, respectively. These orbital energy levels are the weighted average of PDOS in Fig. S2 in the Ref. [40]. Note that the orbital energy levels in FL *w*ZnO have been corrected to eliminate the effect of internal electric field induced by polar surface, as shown in Fig. S3 in the Ref. [40]. The ideal vacuum [48,49] of BK ZnO is set to zero, and the O 2*s*-orbital energy level of FL *g*ZnO (FL *w*ZnO) is aligned to the O 2*s*-orbital energy level of BK *g*ZnO (BK *w*ZnO).

IV. CONCLUSIONS

In conclusion, our first-principles calculations revealed the significant structural transformation of FL ZnO takes place with a thickness of 9–12 Zn-O atomic layers, where thinner than 9 layers, FL ZnO always possesses the graphitic structure, while thicker than 12 layers, FL ZnO prefers the wurtzite structure. When the thickness is 9–12 layers, both graphitic and wurtzite structures can coexist in FL ZnO at room temperature. In FL *g*ZnO, the interlayer interaction is not the van der Waals interaction normally found in layered materials but the long-range Coulomb interaction. And the structural transformation does not alter the charge population of Zn and O inside FL ZnO. We also gave an evident description of the microscopic origin of the structural transformation in FL ZnO, namely, avoiding that the polar surface be dominant, forming the graphitic structure in thin FL ZnO, and avoiding that the high energy of the O $2p_z$ orbital be dominant, forming the wurtzite structure in thick FL ZnO. Our work is helpful to elucidate that the critical thickness for structural transformation is remarkably affected by strain [20,24], substrate [24], and doping [25] from a microscopic perspective, and to guide a clear direction of regulating the structure and further optimizing the electronic properties of FL ZnO for function-advanced stacked 2D devices.

ACKNOWLEDGMENTS

D.H. would like to thank S.-B. Zhang for helpful discussions on the ideal vacuum level of solids and Wei-Quan Tian for helpful discussion on the orbital energy level. This work was supported by the National Natural Science Foundation of China (Grants No. 11974344, No. 12274180, No. 12274172, and No. 11704111) and the Science and Technology Development Plan Project of Jilin Province, China (Grant No. 20230101004JC).

[1] J. S. Liu, C. X. Shan, H. Shen, B. H. Li, Z. Z. Zhang, L. Liu, L. G. Zhang, and D. Z. Shen, Appl. Phys. Lett. **101**, 011106 (2012).

[2] A. Chen, H. Zhu, Y. Wu, M. Chen, Y. Zhu, X. Gui, and Z. Tang, Adv. Funct. Mater. **26**, 3696 (2016).

[3] A. Tsukazaki, A. Ohtomo, T. Onuma, M. Ohtani, T. Makino, M. Sumiya, K. Ohtani, S. F. Chichibu, S. Fuke, Y. Segawa, H. Ohno, H. Koinuma, and M. Kawasaki, Nat. Mater. **4**, 42 (2005).

[4] H. Zhu, C.-X. Shan, B. Yao, B.-H. Li, J.-Y. Zhang, Z.-Z. Zhang, D.-X. Zhao, D.-Z. Shen, X.-W. Fan, Y.-M. Lu, and Z.-K. Tang, Adv. Mater. **21**, 1613 (2009).

[5] H. Zhu, C.-X. Shan, J.-Y. Zhang, Z.-Z. Zhang, B.-H. Li, D.-X. Zhao, B. Yao, D.-Z. Shen, X.-W. Fan, Z.-K. Tang, X. Hou, and K.-L. Choy, Adv. Mater. **22**, 1877 (2010).

[6] U. Özgür, D. Hofstetter, and H. Morkoç, Proc. IEEE **98**, 1255 (2010).

[7] H. Morkoç and U. Özgür, General properties of ZnO, in *Zinc Oxide: Fundamentals, Materials and Device Technology* (Wiley-VCH Verlag GmbH & Co. KGaA, Weinheim, 2009), pp. 1–76.

[8] M. Catti, Y. Noel, and R. Dovesi, J. Phys. Chem. Solids **64**, 2183 (2003).

[9] J. Xin, Y. Zheng, and E. Shi, Appl. Phys. Lett. **91**, 112902 (2007).

[10] A. Segura, J. A. Sans, F. J. Manjón, A. Muñoz, and M. J. Herrera-Cabrera, Appl. Phys. Lett. **83**, 278 (2003).

[11] B. Amrani, I. Chiboub, S. Hiadsi, T. Benmessabih, and N. Hamdadou, Solid State Commun. **137**, 395 (2006).

[12] A. Schleife, F. Fuchs, J. Furthmüller, and F. Bechstedt, Phys. Rev. B **73**, 245212 (2006).

[13] Z. Xin-Yu, C. Zhou-Wen, Q. Yan-Peng, F. Yan, Z. Liang, Q. Li, M. Ming-Zhen, L. Ri-Ping, and W. Wen-Kui, Chin. Phys. Lett. **24**, 1032 (2007).

[14] Z. L. Wang, J. Phys.: Condens. Matter **16**, R829 (2004).

[15] A. B. Djurišić, X. Chen, Y. H. Leung, and A. M. Ching Ng, J. Mater. Chem. **22**, 6526 (2012).

[16] L. Schmidt-Mende and J. L. MacManus-Driscoll, Mater. Today **10**, 40 (2007).

[17] J. Theerthagiri, S. Salla, R. A. Senthil, P. Nithyadharseni, A. Madankumar, P. Arunachalam, T. Maiyalagan, and H.-S. Kim, Nanotechnology **30**, 392001 (2019).

[18] H. Q. Ta, L. Zhao, D. Pohl, J. Pang, B. Trzebicka, B. Rellinghaus, D. Pribat, T. Gemming, Z. Liu, A. Bachmatiuk, and M. H. Rummeli, Crystals **6**, 100 (2016).

[19] C. L. Freeman, F. Claeyssens, N. L. Allan, and J. H. Harding, Phys. Rev. Lett. **96**, 066102 (2006).

[20] D. Wu, M. G. Lagally, and F. Liu, Phys. Rev. Lett. **107**, 236101 (2011).

[21] C. Tusche, H. L. Meyerheim, and J. Kirschner, Phys. Rev. Lett. **99**, 026102 (2007).

[22] J. Lee, D. C. Sorescu, and X. Deng, J. Phys. Chem. Lett. **7**, 1335 (2016).

[23] T. Kumagai, S. Liu, A. Shiotari, D. Baugh, S. Shaikhutdinov, and M. Wolf, J. Phys.: Condens. Matter **28**, 494003 (2016).

[24] L. Lin, Z. Zeng, Q. Fu, and X. Bao, AIP Adv. **10**, 125125 (2020).

[25] H. Sang, Y. Zeng, and L. Sun, Eur. Phys. J. Plus **134**, 24 (2019).

[26] H.-K. Hong, J. Jo, D. Hwang, J. Lee, N. Y. Kim, S. Son, J. H. Kim, M.-J. Jin, Y. C. Jun, R. Erni, S. K. Kwak, J.-W. Yoo, and Z. Lee, Nano Lett. **17**, 120 (2017).

[27] K. B. Tom, S. Lin, L. F. Wan, J. Wang, N. Ahlm, A. T. N'Diaye, K. Bustillo, J. Huang, Y. Liu, S. Lou, R. Chen, S. Yan, H. Wu, D. Jin, H. Yuan, D. Prendergast, and J. Yao, ACS Nano **12**, 7554 (2018).

[28] H. Wu, Q. Fu, Y. Li, Y. Cui, R. Wang, N. Su, L. Lin, A. Dong, Y. Ning, F. Yang, and X. Bao, Nano Res. **12**, 2348 (2019).

[29] N. Mahmood, H. Khan, K. Tran, P. Kuppe, A. Zavabeti, P. Atkin, M. B. Ghasemian, J. Yang, C. Xu, S. A. Tawfik, M. J. S. Spencer, J. Z. Ou, K. Khoshmanesh, C. F. McConville, Y. Li, and K. Kalantar-Zadeh, Mater. Today **44**, 69 (2021).

[30] H. Yu, Q. Liao, Z. Kang, Z. Wang, B. Liu, X. Zhang, J. Du, Y. Ou, M. Hong, J. Xiao, Z. Zhang, and Y. Zhang, Small **16**, 2005520 (2020).

[31] D. Han, X.-B. Li, D. Wang, N.-K. Chen, and X.-W. Fan, Phys. Rev. B **105**, 024104 (2022).

[32] P. Hohenberg and W. Kohn, Phys. Rev. **136**, B864 (1964).

[33] W. Kohn and L. J. Sham, Phys. Rev. **140**, A1133 (1965).

[34] G. Kresse and J. Furthmüller, Comput. Mater. Sci. **6**, 15 (1996).

[35] G. Kresse and J. Furthmüller, Phys. Rev. B **54**, 11169 (1996).

[36] P. E. Blöchl, Phys. Rev. B **50**, 17953 (1994).

[37] J. P. Perdew, K. Burke, and M. Ernzerhof, Phys. Rev. Lett. **77**, 3865 (1996).

[38] J. Klimeš, D. R. Bowler, and A. Michaelides, J. Phys.: Condens. Matter **22**, 022201 (2010).

[39] H. Karzel, W. Potzel, M. Köfferlein, W. Schiessl, M. Steiner, U. Hiller, G. M. Kalvius, D. W. Mitchell, T. P. Das, P. Blaha, K. Schwarz, and M. P. Pasternak, Phys. Rev. B **53**, 11425 (1996).

[40] See Supplemental Material at http://link.aps.org/supplemental/10.1103/PhysRevB.109.014105 for the additional data on the unit cells of BK *g*ZnO and BK *w*ZnO, the density of states and average electrostatic potential of FL ZnO, and the dipole energy of FL *w*ZnO.

[41] G. Henkelman, B. P. Uberuaga, and H. Jónsson, J. Chem. Phys. **113**, 9901 (2000).

[42] R. Dronskowski and P. E. Bloechl, J. Phys. Chem. **97**, 8617 (1993).

[43] V. L. Deringer, A. L. Tchougréeff, and R. Dronskowski, J. Phys. Chem. A **115**, 5461 (2011).

[44] S. Maintz, V. L. Deringer, A. L. Tchougréeff, and R. Dronskowski, J. Comput. Chem. **34**, 2557 (2013).

[45] S. Maintz, V. L. Deringer, A. L. Tchougréeff, and R. Dronskowski, J. Comput. Chem. **37**, 1030 (2016).

[46] R. Nelson, C. Ertural, J. George, V. L. Deringer, G. Hautier, and R. Dronskowski, J. Comput. Chem. **41**, 1931 (2020).

[47] J. Sun, R. C. Remsing, Y. Zhang, Z. Sun, A. Ruzsinszky, H. Peng, Z. Yang, A. Paul, U. Waghmare, X. Wu, M. L. Klein, and J. P. Perdew, Nat. Chem. **8**, 831 (2016).

[48] D.-H. Choe, D. West, and S. Zhang, Phys. Rev. Lett. **121**, 196802 (2018).

[49] Z. Jiang, D. West, and S. Zhang, Phys. Rev. Mater. **7**, 015001 (2023).

[50] K. Momma and F. Izumi, J. Appl. Crystallogr. **44**, 1272 (2011).